Principal Investigators:
Richard Aster aster@ees.nmt.edu
Philip Kyle kyle@nmt.edu
Both at New Mexico Institute of Mining and Technology, Socorro, NM, 87801

Experiment Name: Tomo Erebus

Seismic Tomography of Erebus Volcano, Antarctica

Daria Zandomeneghi[1], Philip Kyle[2], Pnina Miller[3], Catherine Snelson[2], Richard Aster[2]

[1] - International Centre for Theoretical Physics, Trieste, Italy; E-mail: dzandome@ictp.it
[2] - Department of Earth and Environmental Science, New Mexico Institute of Mining and Technology, Socorro
[3] - IRIS PASSCAL Instrument Center, New Mexico Institute of Mining and Technology

Mount Erebus (77°32'S, 167°10'E; elevation 3794 meters) is the most active volcano in Antarctica and is well known for its persistent lava lake. The lake constitutes an "open window" into the conduit and underlying feeding system and offers a rare opportunity to observe a shallow convecting magmatic system.

Imaging and modeling of the internal structure of Erebus volcano are best done through compiling information from arrays of seismometers positioned strategically around the volcano. From these data, the three- dimensional (3-D) structure of the conduit can be pieced together. Building this 3-D model of Erebus was a main goal of the seismic tomographic experiment Tomo Erebus (TE). During the 2007–2008 austral field season, 23 intermediate-period seismometers were installed to contribute data, through the winter, for the passive- source aspect of the experiment. One year later, 100 three- component short-period stations were deployed to record 16 chemical blasts (see Figure 1).

These networks will help scientists update older 2- D models of the magmatic system underlying the lava lake [Dibble et al., 1994] with 3-D interpretations. Such studies will greatly assist scientists in their understanding of the dimensions, position, and complexity of the conduit and magmatic system. Further, knowledge of the physical makeup of the volcano's edifice will help to generate a unified model of Erebus volcano and to solve questions about the mechanism, location, and generation of magma convection and seismic signals.

Experimental and Geological Context

Erebus volcano, located just off the Ross Ice Shelf on Ross Island, is a perfect, natural laboratory for seismology, with very low seismic noise, an absence of human disturbances, ease of access, and a wide range of seismic signals (including explosions, tremor, and long- and very-long-period seismic activity). Eruptive activity at Erebus has been monitored since 1980 with a short-period seismic network and since 2003 with broadband seismometers and associated instruments (e.g., infrasound and Global Positioning System (GPS) receivers; tilt-meters; and video, thermal, and meteorological sensors [see Aster et al., 2004]). Ongoing multidisciplinary studies of Erebus [Oppenheimer and Kyle, 2008] evidence the complexity of the volcano's evolution.

These studies have revealed that the Erebus stratovolcano began forming 1.3 million years ago as part of the larger Erebus volcanic province, at the south end of the Terror rift (an intraplate rift that is a major arm of the West Antarctic rift). Seismic studies suggest that the mantle beneath Erebus is 150–200 (±100) kelvins hotter than its surroundings, showing the existence of a thermal anomaly under the region [Watson et al., 2006]. The surface expression of this thermal anomaly is a lava lake that is phonolitic, meaning that the magma feeding Mount Erebus is alkaline rich, a factor indicative of intraplate magmatism.

Tomo Erebus Setup:Determining Seismic Array Geometry

The goals of TE are to obtain a P wave 2- D velocity profile for Ross Island and a 3-D velocity model for the Erebus summit. The 3-D velocity model will apply the tomography code of Toomey et al. [1994], already used in local active- source seismic tomography experiments at mid-ocean ridges and volcanic islands [e.g., Zandomeneghi et al., 2009]. This method, based on P wave travel times, exploits a shortest- time ray tracing and a least squares algorithm inversion. An advantage of the code is that it takes into account even steep topography, allowing scientists to model seismic ray propagation and velocity in fine detail.

Prior to fieldwork, the code was run to test different code parameters and to establish the optimal geometry for shots and receivers such that scientists could best image the volcano's structure. The synthetic tests consisted of assuming different configurations of sources and receivers in a known 3-D velocity model. After calculating the travel times for each setting, the obtained data set was inverted and the final velocity structure was compared with the known model. Good performance was shown when virtual nodes within the model were spaced 50 meters apart to optimize ray tracing and 100 meters apart to fine tune velocity signatures. From this array of virtual nodes, different geometries for stations and shots were tested. On the basis of this, scientists decided to deploy 100 stations specifically meant to image the structure of Erebus in 3-D over 9 square kilometers, with an interstation distance of 350–500 meters.

Tomo Erebus Experiment

During the 2007–2008 austral summer season, 23 intermediate-period three-component seismic sensors (natural frequency 30 seconds to 100 hertz) were deployed for the passive portion of the experiment. These sensors recorded natural seismic activity during the 2008 winter. To prepare for the harsh and isolated conditions of winter, seismic stations were specially designed by the Incorporated Research Institutions for Seismology (IRIS) Program for Array Seismic Studies of the Continental Lithosphere (PASSCAL) Instrument Center for Antarctic weather conditions (http://www.passcal.nmt.edu/Polar/index.html). For each station this design included a 24-bit data acquisition system (DAS, with a sampling rate of 40 samples per second), a solar power controller, and batteries specifically designed for long life housed in insulated boxes. Each station also included a GPS antenna and two 65-watt solar panels mounted on reinforced aluminum frames.

The 2007–2008 fieldwork also provided an opportunity to scope out where the active seismic experiment would take place during the following summer season. Using chemical blasts as seismic sources, because natural seismic activity is low and the Antarctic summer field season is short, scientists tested three trial locations. Armed with these data, scientists in the 2008–2009 summer field season split their work into two separate experiments (Figure 1): TE-2D and TE- 3D. In TE-2D, scientists deployed 21 seismometers along a 90- kilometer- long east-west line across Ross Island, using three chemical blasts to image the 2- D deep structure of the region. One shot each was positioned at both ends of the array, and a third shot was placed in the array's middle.

In TE- 3D, scientists arranged 79 seismometers in a 3- × 3- kilometer grid centered on the summit crater to obtain a 3-D model of the conduit and of the upper few kilometers beneath the lava lake. One hundred short- period three- component sensors (4.5 hertz) were used to collect data for TE-2D and TE-3D, with a sampling rate of 200 samples per second. These short-period stations held one 10-watt solar panel and either a 58- or 32- ampere- hour gel- cell battery. The same IRIS setup of insulated boxes was used, although the solar panel and GPS antenna were mounted directly on top of the boxes for the TE- 3D stations. The 13 shots for TE-3D were azimuthally distributed to provide optimal seismic ray path coverage (Figure 1).

The blasts themselves were made by first drilling holes 20 centimeters in diameter in snow and ice to depths of 7–15 meters. After being loaded with explosives, the holes were stemmed with snow and left at least 24 hours to sinter. Scientists used an ammonium nitrate and fuel oil mixture (ANFO) with pentolite boosters (a mixture of pentaerythritol tetranitrate and trinitrotoluene) for blasting with detonation cord and seismic detonators. Shots ranged in size between 75 and 230 kilograms for the 2007–2008 tests and between 75 and 600 kilograms in 2008–2009. Dynamite was used for a shot in McMurdo Sound. Shot locations were determined using dual-frequency GPS receivers with differential methods.

Data Analysis to Build a Model of Erebus's Conduit

In a preliminary examination of DAS data and log files, which describe each station's state of health, GPS performance, power input, sensor channel centering, and timing errors, only very few pieces of data were found to be missing, presumably due to malfunctions of instruments. Shots for TE-3D were recorded over the entire summit array and some of the flank stations with very low noise (see Figure S1 in the electronic supplement to this Eos issue (http://www.agu.org/eos _elec/)). Shot records of TE-2D are more uncertain, but most stations on the east side of the line deployment recorded the westernmost shot with high quality. Initial data analysis indicates that waveforms and frequencies of signals recorded vary across the network, suggesting medium heterogeneity. Nonetheless, the first arrival times of P waves should be identifiable with small uncertainty, helping to better model the traveltime information.

Data recorded by the stations installed in 2007–2008 for passive seismic analysis will be introduced in this tomography to increase lateral resolution and modeled depth. In addition, it is hoped that the 2-D data will help to delineate the presence of major velocity anomalies related to the thermal imprint of what may be wide- scale mantle unconformity. Because of its higher resolution, TE-3D is expected to image the presence of hectometer- scale velocity perturbations in the first 2 kilometers of the volcano edifice, due to volcanic deposits, thermal anomalies, geochemically altered rocks, and magma bodies. Both 2-D and 3-D data will help scientists better understand the regional tectonics and its local volcanic implications.

Acknowledgments

The United States Antarctic Program, Raytheon Polar Services Company, Ice Core and Drilling Services (based at the University of Wisconsin– Madison), and the IRIS PASSCAL Instrument Center provided invaluable assistance to this project. Names and affiliations of the many people, teams, and organizations that also helped with TE are available at http://erebus.nmt.edu/Geophysics/Active_Source_Tomo.html. This work was supported by the Office of Polar Programs, U.S.National Science Foundation.

References:

Aster, R., et al. (2004), Real- time data received from Mount Erebus volcano, Antarctica, Eos Trans. AGU, 85(10), 97, 100–101.

Dibble, R. R., B. O'Brien, and C. A. Rowe (1994), The velocity structure of Mount Erebus, Antarctica, and its lava lake, in Volcanological and Environmental Studies of Mount Erebus, Antarctica, Antarct. Res. Ser., vol. 66, edited by P. Kyle, pp. 1–16, AGU, Washington, D. C.

Oppenheimer, C., and P. Kyle (Eds.) (2008), Volcanology of Erebus volcano, Antarctica, J. Volcanol. Geotherm. Res., 177(3), 224 pp.

Toomey, D. R., S. C. Solomon, and G. M. Purdy(1994), Tomographic imaging of the shallow crustal structure of the East Pacific Rise at 9°30’N, J. Geophys. Res., 99(B12), 24,135–24,157.

Watson, T., A. Nyblade, D. A. Wiens, S. Anandakrishnan, M. Benoit, P. J. Shore, D. Voigt, and J. VanDecar (2006), P and S velocity structure of the upper mantle beneath the Transantarctic Mountains, East Antarctic craton, and Ross Sea from travel time tomography, Geochem. Geophys. Geosyst., 7, Q07005, doi:10.1029/2005GC001238.

Zandomeneghi, D., A. Barclay, J. Almendros, J. M. Ibañez, W. S. D. Wilcock, and T. Ben-Zvi (2009), Crustal structure of Deception Island volcano from P wave seismic tomography: Tectonic and volcanic implications, J. Geophys. Res., 114, B06310, doi:10.1029/2008JB006119.

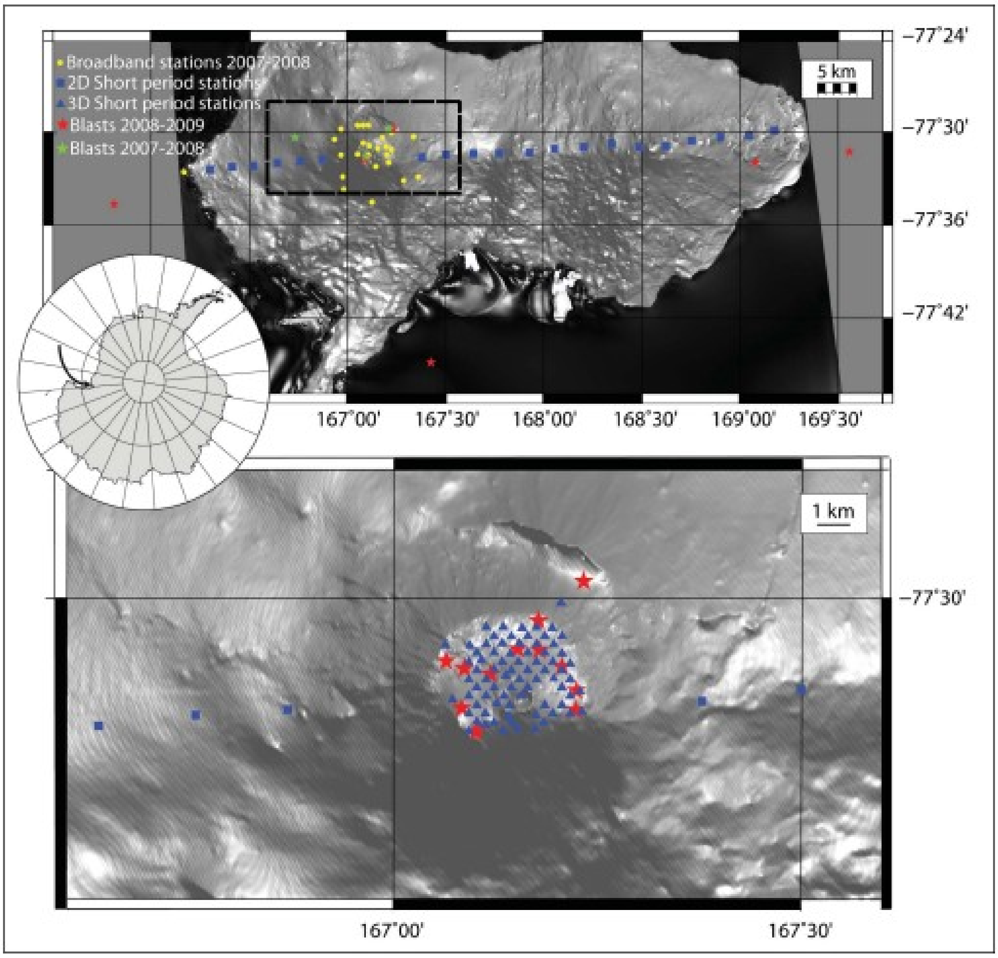

Fig. 1. Top map and inset show Ross Island and the experiment configuration for the 2007–2008 and 2008–2009 field seasons. Bottom image shows a close-up of the locations of instruments deployed on Mount Erebus's summit.

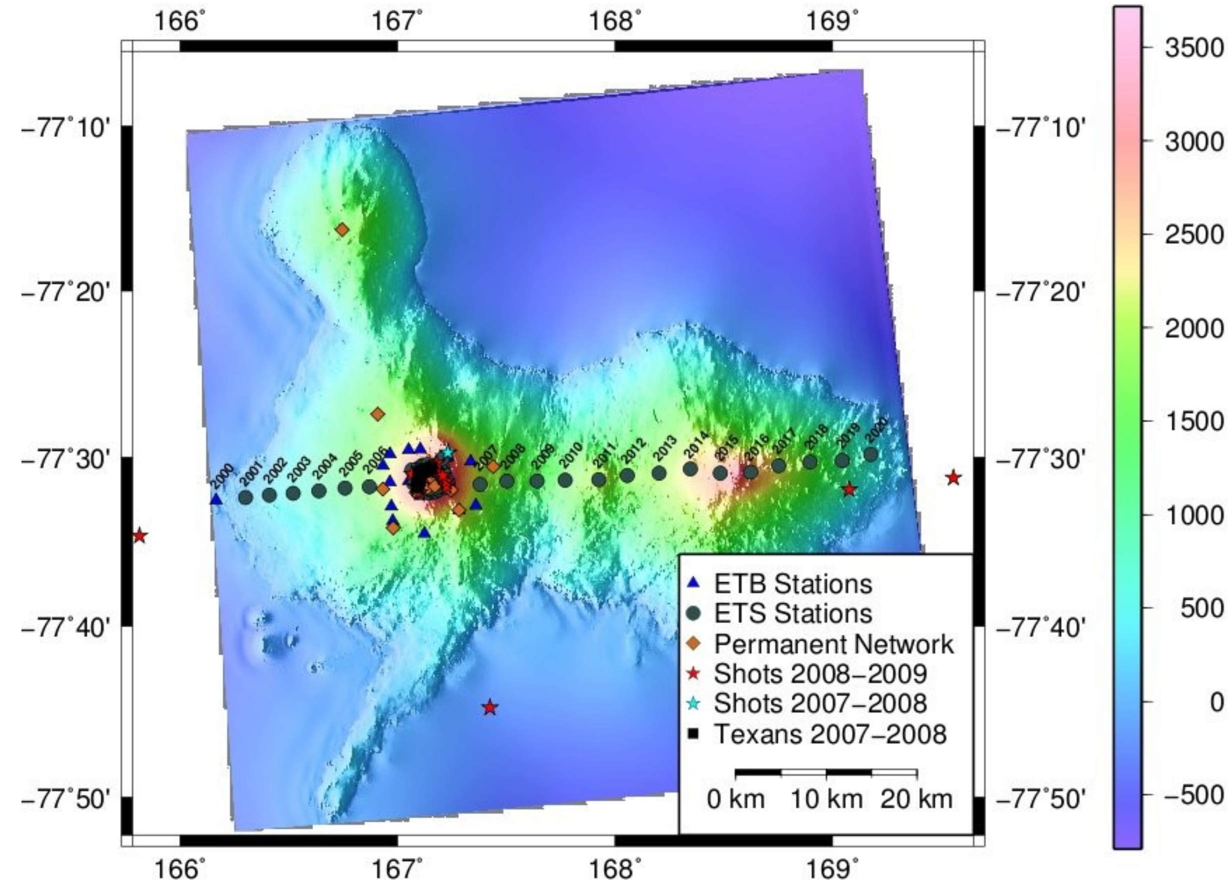

Figure 2: Map of Ross Island showing all stations and shots from the 2007-2008, and 2008-2009 field seasons.

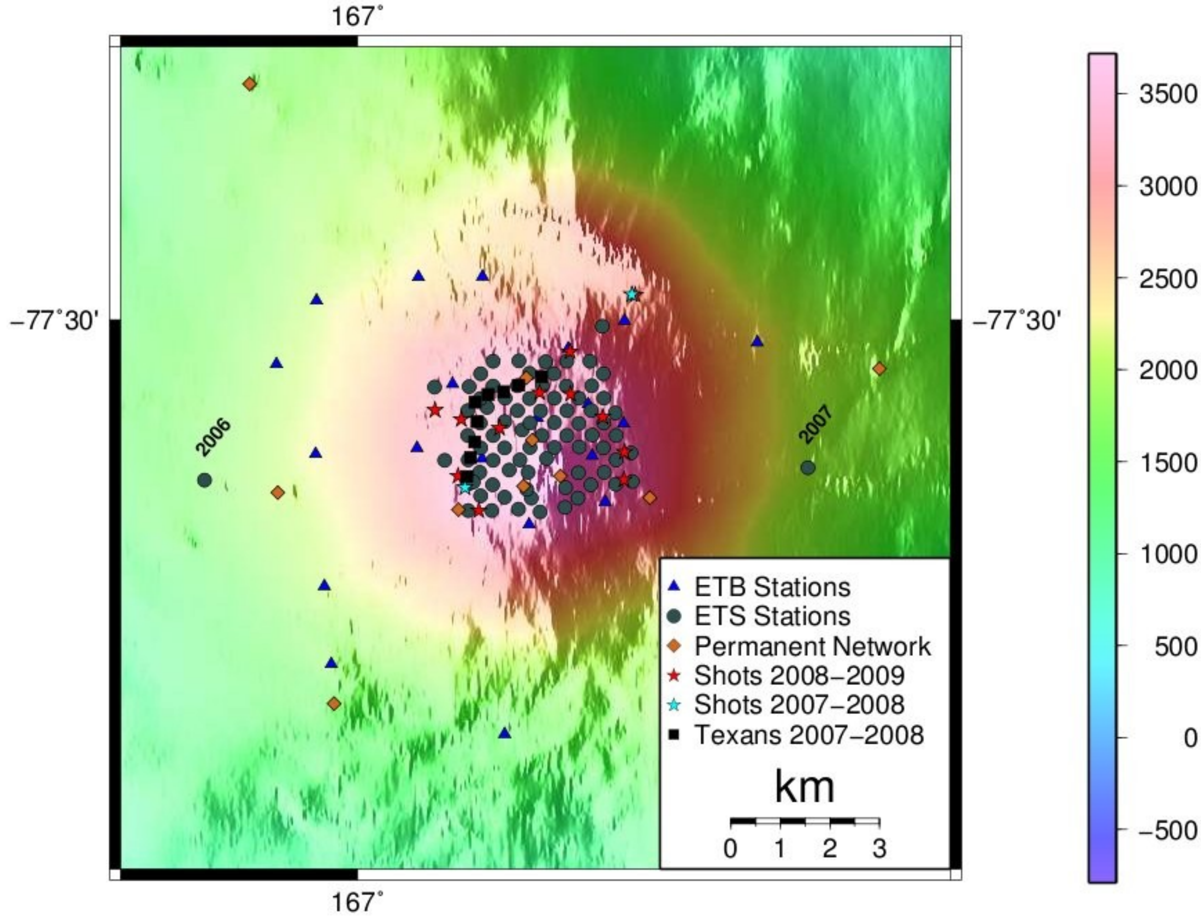

Figure 3: Close up of the summit showing all stations and shots from the 2007-2008 and 2008-2009 field seasons.

Shot Point ID	Shot Point Name	Time (UTC) yyyy:jd:hr:mn:ss	latitude (WGS84)	longitude (WGS84)	elevation (m)	type of source	size (kg)	depth below surface (m)	# of holes
4000	Windless Bight	2008:346:01:40:00	77.74667	167.42534	38.774	ANFO	500	15	4
4001	Cape Crozier	2008:346:00:17:00	77.52047	169.55677	23.408	ANFO	600	14.5	5
4002	Cape Royd	2008:345:05:17:00	77.57793	165.81121	-0.123	dynamite	200	water	1
4003	Crozier 2	2008:357:02:27:00	77.53207	169.07915	792.162	ANFO	500	15	5
4004	FANG	2008:355:21:51:00	77.49550	167.23412	2928.494	ANFO	300	15	3
4005	Cones2	2008:356:09:00:00	77.53486	167.10207	3494.562	ANFO	100	6.0, 6.13, 7.4	3
4006	Cones	2008:356:08:23:00	77.52857	167.08469	3439.634	ANFO	200	14.9	2
4007	CORR13	2008:356:07:50:00	77.51817	167.08751	3294.538	ANFO	75	20	1
4008	Tramsw 2	2008:356:09:45:00	77.51977	167.11968	3421.712	ANFO	75	6.15, 6.8	2
4009	Sunshine Valley CornerSW	2008:359:00:30:00	77.51650	167.06509	3225.665	ANFO	100	5.5, 5.8, 7.9	3
4010	HoleH	2008:358:20:55:00	77.51334	167.15366	3424.817	ANFO	75	7.8, 8.15	2
4011	Stinky (13)	2008:358:23:49:00	77.51361	167.17945	3424.82	ANFO	75	8.1, 8.5	2
4012	Black (19)	2008:357:05:02:00	77.52920	167.22458	3461.882	ANFO	100	7.5	2
4013	Tower (17)	2008:357:05:28:00	77.52416	167.22520	2928.494	ANFO	100	7.8, 8.7	2
4014	Fog (15)	2008:357:05:55:00	77.51781	167.20687	3466.01	ANFO	100	8.0, 8.6	2
4015	Stuck (11)	2008:358:23:27:00	77.50585	167.17907	3351.054	ANFO	100	6.2 7.1	2

Receiver ID	latitude (WGS84)	longitude (WGS84)	Elevation (m)	Serial # of data logger	data logger manufacturer	data logger model #	sensor manufacturer	sensor model number
1001	-77.5245	166.964417	2359	9297	RefTek	RT-130	Guralp	40-T
1002	-77.548567	166.97205	2114	9892	RefTek	RT-130	Guralp	40-T
1003	-77.508133	166.931617	2001	9866	RefTek	RT-130	Guralp	40-T
1004	-77.4965	166.965167	2143	9873	RefTek	RT-130	Guralp	40-T
1005	-77.492167	167.051167	2452	9848	RefTek	RT-130	Guralp	40-T
1006	-77.492083	167.105167	2583	9915	RefTek	RT-130	Guralp	40-T
1007	-77.5628	166.9777	1780	995F	RefTek	RT-130	Guralp	40-T
1008	-77.504183	167.336983	2495	990B	RefTek	RT-130	Guralp	40-T
1009*	-77.542717	166.1646	16	995D	RefTek	RT-130	Guralp	40-T
1010	-77.55235	167.282717	2361	92C8	RefTek	RT-130	Guralp	40-T
1011	-77.517917	167.151567	3494	976C	RefTek	RT-130	Guralp	40-T
1012	-77.515117	167.109217	3373	985B	RefTek	RT-130	Guralp	40-T
1013	-77.547933	167.360350	1979	9868	RefTek	RT-130	Guralp	40-T
1014	-77.515417	167.194300	3437	944B	RefTek	RT-130	Guralp	40-T
1015	-77.537333	167.144517	3405	9859	RefTek	RT-130	Guralp	40-T
1016	-77.511700	167.079967	3274	92D9	RefTek	RT-130	Guralp	40-T
1017	-77.533283	167.208633	3437	995A	RefTek	RT-130	Guralp	40-T
1018	-77.524883	167.197683	3566	995B	RefTek	RT-130	Guralp	40-T
1019	-77.505250	167.177533	3290	988F	RefTek	RT-130	Guralp	40-T
1020	-77.525333	167.104700	3493	953B	RefTek	RT-130	Guralp	40-T
1021	-77.500167	167.225217	2951	984D	RefTek	RT-130	Guralp	40-T
1022	-77.518967	167.224267	3455	9920	RefTek	RT-130	Guralp	40-T
1023	-77.523383	167.050150	3236	9343	RefTek	RT-130	Guralp	40-T
1024	-77.575517	167.124017	1540	9876	RefTek	RT-130	Guralp	40-T

* Sensor changed to Mark Products L-28 on November 10th 2008.

Receiver ID	latitude (WGS84)	longitude (WGS84)	Elevation (m)	serial # of data logger	data logger manufacturer	data logger model #	sensor manufacturer	sensor model number
2001	-77.53994	166.30038	173	9777	RefTek	RT-130	Mark Products	L-28
2002	-77.53737	166.40999	398	9142	RefTek	RT-130	Mark Products	L-28
2003	-77.5357	166.52064	633	9095	RefTek	RT-130	Mark Products	L-28
2004	-77.53352	166.63891	921	9914	RefTek	RT-130	Mark Products	L-28
2005	-77.53053	166.75738	1242	9805	RefTek	RT-130	Mark Products	L-28
2006	-77.52926	166.87078	1680	9553	RefTek	RT-130	Mark Products	L-28
2007	-77.52702	167.37993	2091	9310	RefTek	RT-130	Mark Products	L-28
2008	-77.52374	167.50133	1786	949A	RefTek	RT-130	Mark Products	L-28
2009	-77.52338	167.64172	1491	9811	RefTek	RT-130	Mark Products	L-28
2010	-77.5225	167.77194	1583	9260	RefTek	RT-130	Mark Products	L-28
2011	-77.52202	167.92625	2048	92D5	RefTek	RT-130	Mark Products	L-28
2012	-77.51818	168.05618	1808	938B	RefTek	RT-130	Mark Products	L-28
2013	-77.51552	168.204	2007	92B4	RefTek	RT-130	Mark Products	L-28
2014	-77.51165	168.34747	2501	9844	RefTek	RT-130	Mark Products	L-28
2015	-77.51547	168.48471	2925	92BE	RefTek	RT-130	Mark Products	L-28
2016	-77.51452	168.62449	2860	924C	RefTek	RT-130	Mark Products	L-28
2017	-77.50844	168.75416	2317	92D1	RefTek	RT-130	Mark Products	L-28
2018	-77.50433	168.89784	1841	9342	RefTek	RT-130	Mark Products	L-28
2019	-77.50288	169.0452	1346	9099	RefTek	RT-130	Mark Products	L-28
2020	-77.4971	169.17777	643	913F	RefTek	RT-130	Mark Products	L-28
3021	-77.5099	167.16557	3390	978F	RefTek	RT-130	Mark Products	L-28
3022	-77.50983	167.14503	3394	978A	RefTek	RT-130	Mark Products	L-28
3023	-77.5121	167.13493	3387	9874	RefTek	RT-130	Mark Products	L-28
3024	-77.51435	167.12445	3366	929D	RefTek	RT-130	Mark Products	L-28
3025	-77.51212	167.11406	3342	92D6	RefTek	RT-130	Mark Products	L-28
3026	-77.51659	167.093	3345	9240	RefTek	RT-130	Mark Products	L-28
3027	-77.50987	167.20732	3361	92A4	RefTek	RT-130	Mark Products	L-28
3028	-77.51208	167.19729	3382	9828	RefTek	RT-130	Mark Products	L-28
3030	-77.52112	167.09288	3383	9896	RefTek	RT-130	Mark Products	L-28
3031	-77.51889	167.10345	3377	945A	RefTek	RT-130	Mark Products	L-28
3032	-77.51606	167.10916	3375	9140	RefTek	RT-130	Mark Products	L-28
3033	-77.51213	167.1762	3399	92EA	RefTek	RT-130	Mark Products	L-28
3034	-77.51207	167.15577	3408	92F0	RefTek	RT-130	Mark Products	L-28
3035	-77.51439	167.14486	3417	92E4	RefTek	RT-130	Mark Products	L-28
3036	-77.51661	167.13501	3421	92A0	RefTek	RT-130	Mark Products	L-28
3037	-77.51859	167.12402	3446	9780	RefTek	RT-130	Mark Products	L-28
3038	-77.52116	167.11426	3449	92E2	RefTek	RT-130	Mark Products	L-28
3039	-77.52344	167.12413	3573	92A5	RefTek	RT-130	Mark Products	L-28
3040	-77.52567	167.11426	3539	92C9	RefTek	RT-130	Mark Products	L-28
3041	-77.52791	167.1031	3512	9261	RefTek	RT-130	Mark Products	L-28
3042	-77.53006	167.09288	3512	9559	RefTek	RT-130	Mark Products	L-28
3043	-77.52342	167.10374	3456	91F7	RefTek	RT-130	Mark Products	L-28
3044	-77.52564	167.09313	3454	9917	RefTek	RT-130	Mark Products	L-28
3045	-77.51438	167.20756	3412	9294	RefTek	RT-130	Mark Products	L-28
3046	-77.51662	167.19693	3456	9290	RefTek	RT-130	Mark Products	L-28
3047	-77.51894	167.18651	3516	9283	RefTek	RT-130	Mark Products	L-28
3048	-77.51657	167.17658	3468	983D	RefTek	RT-130	Mark Products	L-28
3049	-77.51435	167.16609	3429	9803	RefTek	RT-130	Mark Products	L-28
3050	-77.51434	167.18666	3425	9912	RefTek	RT-130	Mark Products	L-28

3051	-77.51882	167.16587	3519	9869	RefTek	RT-130	Mark Products	L-28
3052	-77.52333	167.16593	3699	944C	RefTek	RT-130	Mark Products	L-28
3053	-77.52119	167.17656	3591	9241	RefTek	RT-130	Mark Products	L-28
3054	-77.51892	167.20757	3480	983E	RefTek	RT-130	Mark Products	L-28
3055	-77.52118	167.21802	3481	91E5	RefTek	RT-130	Mark Products	L-28
3056	-77.52329	167.18687	3607	990D	RefTek	RT-130	Mark Products	L-28
3057	-77.51702	167.21719	3446	92F7	RefTek	RT-130	Mark Products	L-28
3058	-77.52345	167.20699	3544	9891	RefTek	RT-130	Mark Products	L-28
3059	-77.52105	167.19776	3547	9446	RefTek	RT-130	Mark Products	L-28
3060	-77.51439	167.10342	3354	924A	RefTek	RT-130	Mark Products	L-28
3061	-77.51672	167.15409	3477	9864	RefTek	RT-130	Mark Products	L-28
3062	-77.52016	167.13886	3548	9512	RefTek	RT-130	Mark Products	L-28
3063	-77.5189	167.14537	3515	947D	RefTek	RT-130	Mark Products	L-28
3064	-77.52115	167.15534	3604	9491	RefTek	RT-130	Mark Products	L-28
3065	-77.52562	167.13679	3633	947A	RefTek	RT-130	Mark Products	L-28
3066	-77.52785	167.14371	3712	924E	RefTek	RT-130	Mark Products	L-28
3067	-77.50768	167.15874	3384	9453	RefTek	RT-130	Mark Products	L-28
3068	-77.53487	167.0934	3452	930A	RefTek	RT-130	Mark Products	L-28
3069	-77.53218	167.10373	3527	9461	RefTek	RT-130	Mark Products	L-28
3070	-77.52748	167.12784	3642	995C	RefTek	RT-130	Mark Products	L-28
3071	-77.53011	167.11364	3556	9466	RefTek	RT-130	Mark Products	L-28
3072	-77.53485	167.113	3469	9238	RefTek	RT-130	Mark Products	L-28
3073	-77.50758	167.17648	3360	9292	RefTek	RT-130	Mark Products	L-28
3074	-77.50765	167.19571	3349	990F	RefTek	RT-130	Mark Products	L-28
3075	-77.50758	167.11426	3313	92A1	RefTek	RT-130	Mark Products	L-28
3076	-77.50991	167.10369	3320	92DD	RefTek	RT-130	Mark Products	L-28
3077	-77.53509	167.15373	3518	929B	RefTek	RT-130	Mark Products	L-28
3078	-77.53423	167.17502	3511	9293	RefTek	RT-130	Mark Products	L-28
3079	-77.5324	167.12409	3557	9334	RefTek	RT-130	Mark Products	L-28
3080	-77.5346	167.13564	3521	9791	RefTek	RT-130	Mark Products	L-28
3081	-77.53256	167.14668	3626	980E	RefTek	RT-130	Mark Products	L-28
3082	-77.50983	167.12429	3529	986C	RefTek	RT-130	Mark Products	L-28
3083	-77.51224	167.09409	3331	9C30	RefTek	RT-130	Mark Products	L-28
3084	-77.51233	167.06478	3235	943F	RefTek	RT-130	Mark Products	L-28
3085	-77.52435	167.23053	3458	9924	RefTek	RT-130	Mark Products	L-28
3086	-77.52793	167.18616	3601	9462	RefTek	RT-130	Mark Products	L-28
3087	-77.53258	167.1859	3515	9237	RefTek	RT-130	Mark Products	L-28
3088	-77.53063	167.17526	3627	9926	RefTek	RT-130	Mark Products	L-28
3089	-77.50752	167.13603	3369	9245	RefTek	RT-130	Mark Products	L-28
3090	-77.53096	167.14265	3678	9009	RefTek	RT-130	Mark Products	L-28
3091	-77.52572	167.07326	3426	956F	RefTek	RT-130	Mark Products	L-28
3092	-77.52332	167.14515	3658	925D	RefTek	RT-130	Mark Products	L-28
3093	-77.52562	167.21814	3494	92F4	RefTek	RT-130	Mark Products	L-28
3094	-77.52788	167.20786	3515	909A	RefTek	RT-130	Mark Products	L-28
3095	-77.53015	167.19658	3527	9560	RefTek	RT-130	Mark Products	L-28
3096	-77.53007	167.2178	3488	92C4	RefTek	RT-130	Mark Products	L-28
3097	-77.52956	167.23168	3439	92AC	RefTek	RT-130	Mark Products	L-28
3098	-77.52537	167.15936	3654	991C	RefTek	RT-130	Mark Products	L-28
3099	-77.50123	167.20651	3037	92AB	RefTek	RT-130	Mark Products	L-28